Geophys. J. R. astr. Soc. (1979) **56**, 283–308

The influence of upper mantle discontinuities on the toroidal free oscillations of the Earth

Brian Kennett *Department of Applied Mathematics and Theoretical Physics, University of Cambridge, Silver Street, Cambridge CB3 9EW*

Guust Nolet *Vening Meinesz Laboratorium, Rijksuniversiteit te Utrecht, Lucas Bolwerk 7, Utrecht 2501, The Netherlands*

Received 1978 June 16

Summary. In the simplest approximation the high-frequency toroidal mode dispersion is simply related to the intercept time $\tau_\beta(p)$ as a function of slowness p derived from *SH*-wave travel times. Velocity and density gradients in the Earth introduce perturbations to this simple relation. More pronounced effects arise when the mantle contains discontinuities in elastic properties and these disrupt the regular spacing of eigenfrequencies with radial order at fixed slowness p, a 'solotone' effect. A simple iterative approach is introduced which enables the solotone effect to be calculated for an earth model with multiple discontinuities. At fixed frequency the discontinuities give rise to a distinctive pattern with varying slowness, particularly in the group velocity behaviour. The perturbations due to the discontinuities depend on the reflection coefficients at these interfaces and so are large for modes with slownesses corresponding to turning points near the discontinuities. For mode phase velocities greater than 9 km/s the details of the solotone perturbation are dominated by beating between the effects of different discontinuities.

The theoretical results are illustrated by computations for model 1066B, both directly and using the asymptotic approach. This allows an assessment of the influence of velocity gradients and upper mantle discontinuities on the dispersion. Also the sources of systematic error in Brune's approach to determining toroidal mode dispersion are discussed and bounds on the errors estimated from the calculations.

1 Introduction

Many models of the velocity distribution in the upper mantle of the Earth contain discontinuities in velocity or very strong velocity gradient zones which will approximate discontinuities for low-frequency waves. For low angular order toroidal modes Anderssen & Cleary (1974), Lapwood (1975), Wang, Gettrust & Cleary (1977) and Anderssen (1977) have related the asymptotic spacing of the frequency spectrum with radial order to the radial

travel times of *SH* waves through the whole mantle. They have demonstrated that discontinuities in velocity give rise to a 'solotone' effect of perturbations in the regular asymptotic frequency spacing.

A similar regularity in the spacing of eigenfrequencies, but at fixed slowness, can be derived for a smooth mantle (Pekeris 1965) by essentially a WKBJ approximation. For radial order n the eigenfrequency at fixed slowness p is now simply related to the intercept time $\tau_\beta(p)$ for *SH* body waves by

$$\tfrac{1}{2}\omega_{nl}\tau_\beta(p) = (n + \tfrac{1}{4})\pi$$

for a turning point in the mantle. This result has been used by Nolet & Kennett (1978) in a study of the correspondence between pulse formation by addition of normal modes and multiply reflected phases (*SS*, *SSS* etc.).

Woodhouse (1978) has presented a convenient asymptotic approach to the study of elastic wave propagation in piecewise smooth velocity models. This approach has been employed by Kennett & Woodhouse (1978) to consider the asymptotic behaviour of spheroidal modes whose displacements are confined to the mantle and also the inversion of high-frequency spheroidal modes.

In this paper we present a detailed study of the effects of one or more discontinuities on the high-frequency behaviour of the toroidal modes for arbitrary slowness (p) on the Woodhouse (1978) approach. As in Kennett & Woodhouse (1978) we are able to relate the effects of velocity gradients and discontinuities to additional frequency-dependent phase shifts $\Psi(\omega, p)$ in the dispersion relation

$$\tfrac{1}{2}\omega_{nl}\tau_\beta(p) = (n + \tfrac{1}{4})\pi + \Psi(\omega, p).$$

We introduce a simple iterative approach to the calculation of toroidal mode dispersion in the presence of multiple discontinuities. The 'solotone' contributions from the discontinuities depend on the reflection coefficients at these interfaces and thus are large for modes with slownesses appropriate to ray turning points in the neighbourhood of the discontinuity. For turning points in the lower mantle and for *ScS* equivalent modes the details of the phase shift are dominated by beating effects due to the interaction of contributions from several interfaces. The existence of the 'solotone' effect leads to oscillatory behaviour in the group velocity for fixed mode phase velocity whereas in the simplest treatment the group velocity would be constant.

We compare direct calculations of mode dispersion for model 1066B (Gilbert & Dziewonski 1975) for radial orders up to 29 and angular orders out to 700 with our asymptotic results. This enables us to assess the influence of the upper mantle discontinuities on the overall solotone phase shift, and to examine the significance of velocity and density gradients in the model. In addition we are able to estimate bounds on the systematic errors arising in Brune's (1964) approach to the calculation of toroidal dispersion, from the neglect of discontinuity contributions.

The size of the overall phase shift Ψ is a rather useful measure of the information content in the toroidal modes. When Ψ is large the density has a significant influence on the frequencies of the normal modes, but when Ψ is small the dispersion information is equivalent to that attainable by ray theory.

2 An asymptotic development for toroidal modes

Woodhouse (1978) has presented a systematic account of an asymptotic development of wave propagation in media with smoothly varying velocity profiles. We shall use his

approach to re-derive the simple results of Nolet & Kennett (1978) and to examine the influence of velocity gradients and discontinuities on the toroidal mode spectrum.

The displacement field for a toroidal mode takes the form

$$u_\theta = W(r)\frac{1}{\sin\theta}\frac{\partial}{\partial\phi}Y_l^m(\theta,\phi)\exp(i\omega t), \quad u_\theta = W(r)\frac{\partial}{\partial\theta}Y_l^m(\theta,\phi)\exp(i\omega t), \tag{1}$$

with stresses

$$\tau_{r\theta} = T(r)\frac{1}{\sin\theta}\frac{\partial}{\partial\phi}Y_l^m(\theta,\phi)\exp(i\omega t), \quad \tau_{r\phi} = T(r)\frac{\partial}{\partial\theta}Y_l^m(\theta,\phi)\exp(i\omega t), \tag{2}$$

and

$$Y_l^m(\theta,\phi) = (-1)^m\left[\frac{(l-m)!}{(l+m)!}\right]^{1/2}P_l^m(\cos\theta)\exp(im\phi). \tag{3}$$

The stress and displacement scalars are related by

$$\frac{d}{dr}\begin{pmatrix} W \\ \omega^{-1}T \end{pmatrix} = \omega\begin{pmatrix} r^{-1}\omega^{-1} & \mu^{-1} \\ r^{-2}p^2\mu - \rho - 2r^{-2}\mu\omega^{-2} & -3r^{-1}\omega^{-1} \end{pmatrix}\begin{pmatrix} W \\ \omega^{-1}T \end{pmatrix}, \tag{4}$$

in terms of the slowness $p = [l(l+1)]^{1/2}/\omega = L/\omega$, and the boundary conditions for toroidal modes are

$$\begin{aligned} &T(a) = 0 \quad \text{at the free surface } r = a, \\ &\text{and} \\ &T(b) = 0 \quad \text{at the core–mantle interface } r = b. \end{aligned} \tag{5}$$

At any internal interface (W, T) are continuous.

We will consider the high-frequency limit of the equations (4) for fixed slowness and thus variable large angular order. Woodhouse (1978) has shown that an asymptotic fundamental matrix solution $\mathbf{F}_T$ of (4) (i.e. with both columns asymptotic solutions of (4)) can be written as

$$\mathbf{F}_T = r^{-1}\mathbf{R}(\mathbf{I} + \omega^{-1}r\mathbf{T})\mathbf{E}_\beta, \tag{6}$$

where

$$\mathbf{R} = \begin{pmatrix} 0 & \mu^{-1/2} \\ \mu^{1/2} & 0 \end{pmatrix}. \tag{7}$$

The matrix $\mathbf{T}$ arises from the S-wave velocity (β) and density (ρ) gradients in the model and has the form

$$\mathbf{T} = \begin{pmatrix} 0 & z - q_\beta^2 y \\ y & 0 \end{pmatrix}, \tag{8}$$

and we will usually set $x = z - q_\beta^2 y$. The detailed forms of y and x are given in the Appendix. The phase matrix $\mathbf{E}_\beta$ depends on Airy functions

$$\mathbf{E}_\beta = \pi^{1/2}\begin{pmatrix} \omega^{-1/6}|\partial r\phi_\beta|^{1/2}\,\mathrm{Ai}'(-\omega^{2/3}\phi_\beta) & \omega^{-1/6}|\partial r\phi_\beta|^{1/2}\,\mathrm{Bi}'(-\omega^{2/3}\phi_\beta) \\ -S_\beta\omega^{1/6}|\partial r\phi_\beta|^{-1/2}\,\mathrm{Ai}(-\omega^{2/3}\phi_\beta) & -S_\beta\omega^{1/6}|\partial r\phi_\beta|^{-1/2}\,\mathrm{Bi}(-\omega^{2/3}\phi_\beta) \end{pmatrix}, \tag{9}$$

with

$$q_\beta^2 = (\beta^{-2} - p^2r^{-2}), \quad H_\beta(r) = \int_{R_\beta}^{r}|q_\beta|\,dr,$$

$$\phi_\beta = \mathrm{sgn}(q_\beta^2)\,|\tfrac{3}{2}H_\beta(r)|^{2/3}, \quad s_\beta = \mathrm{sgn}(\partial r\phi_\beta).$$

The radius R_β corresponds to a turning point ($q_\beta = 0$) if one is present in a layer; for regions where the shear velocity increases with depth $s_\beta = 1$. In the subsequent work we assume at most one turning point for the slownesses considered, and to simplify the algebra we follow Kennett & Woodhouse (1978) and write

$$\mathbf{E}_\beta = \begin{pmatrix} \mathrm{Ak}\,(\omega H_\beta) & \mathrm{Bk}\,(\omega H_\beta) \\ -\mathrm{Aj}\,(\omega H_\beta) & -\mathrm{Bj}\,(\omega H_\beta) \end{pmatrix}, \tag{9a}$$

the expressions Aj, Ak, Bj, Bk have simple asymptotic forms (Abramowitz & Stegun 1965). Using the fact that the Wronskian of (Ai, Bi) is π^{-1} the inverse of $\mathbf{E}_\beta$ is

$$\mathbf{E}_\beta^{-1} = \begin{pmatrix} -\mathrm{Bj}\,(\omega H_\beta) & -\mathrm{Bk}\,(\omega H_\beta) \\ \mathrm{Aj}\,(\omega H_\beta) & \mathrm{Ak}\,(\omega H_\beta) \end{pmatrix}. \tag{10}$$

Also in a high-frequency approximation we have

$$(\mathbf{I} + \omega^{-1} r\mathbf{T})^{-1} \simeq (\mathbf{I} - \omega^{-1} r\mathbf{T}) \tag{10a}$$

and so the inverse of the asymptotic fundamental matrix $\mathbf{F}_\mathrm{T}^{-1}$ may easily be constructed using (10) and (10a).

For a region (r_1, r_2) we may factor the propagator matrix for the toroidal modes (Gilbert & Backus 1966) into a product of a fundamental matrix at the top of the shell (r_1) and the inverse of a fundamental matrix at the base of the shell (r_2)

$$\mathbf{P}_\mathrm{T}(r_1, r_2) = \mathbf{F}_\mathrm{T}(r_1)[\mathbf{F}_\mathrm{T}(r_2)]^{-1}. \tag{11}$$

2.1 A SMOOTH MANTLE

The displacement at the Earth's surface can be related to that at the core–mantle boundary by

$$\begin{pmatrix} W(a) \\ 0 \end{pmatrix} = \mathbf{P}_\mathrm{T}(a, b) \begin{pmatrix} W(b) \\ 0 \end{pmatrix} = \mathbf{F}_\mathrm{T}(a)[\mathbf{F}_\mathrm{T}(b)]^{-1} \begin{pmatrix} W(b) \\ 0 \end{pmatrix}, \tag{12}$$

using (11) and the boundary conditions (5). It is convenient to recast (12) into the form

$$\begin{pmatrix} W(a) \\ 0 \end{pmatrix} = \mathbf{F}_\mathrm{T}(a) \begin{pmatrix} c_1 \\ c_2 \end{pmatrix}, \quad \begin{pmatrix} c_1 \\ c_2 \end{pmatrix} = [\mathbf{F}_\mathrm{T}(b)]^{-1} \begin{pmatrix} W(b) \\ 0 \end{pmatrix}, \tag{13}$$

with the new vector $(c_1, c_2)^\mathrm{T}$ depending on the *SH*-wave phase terms at the base of the mantle, from (10),

$$\begin{pmatrix} c_1 \\ c_2 \end{pmatrix} = \begin{pmatrix} -\mathrm{Bk}\,(\omega H_\beta) + \omega^{-1} bx\ \mathrm{Bj}\,(\omega H_\beta) \\ \mathrm{Ak}\,(\omega H_\beta) - \omega^{-1} bx\ \mathrm{Aj}\,(\omega H_\beta) \end{pmatrix} \Bigg|_{r=b} \mu_b^{1/2} b W(b). \tag{14}$$

The asymptotic dispersion relation for the toroidal modes is then obtained from the stress equation in (13) as

$$\frac{\mathrm{Ak}\,(\omega H_\beta) - \omega^{-1} ax\ \mathrm{Aj}\,(\omega H_\beta)}{\mathrm{Bk}\,(\omega H_\beta) - \omega^{-1} ax\ \mathrm{Bj}\,(\omega H_\beta)} \Bigg|_{r=a} = -\frac{c_2}{c_1}. \tag{15}$$

As we would expect we see from (14) that there is in this case complete symmetry in the terms arising from the two boundary conditions.

For a slowness p corresponding to the existence of toroidal modes, $q_\beta^2(a)$ will be positive corresponding to propagating *SH* waves and thus at the surface we may employ the asymptotic approximations for the Airy functions of the type

$$\text{Aj}\,[\omega H_\beta(a)] \sim q_\beta(a)^{-1/2} \cos\,[\omega H_\beta(a) - \pi/4], \tag{16}$$

with R_β set equal to the turning radius at which $q_\beta(r) = 0$, if this lies in the mantle. If we employ the approximations analogous to (16) in (15) we have

$$\tan\,[\omega H_\beta(a) - \pi/4] = \tan\,[\theta(a, R_\beta) - \tan^{-1}(c_2/c_1)],$$

where (17)

$$\theta(a, R_\beta) = \tan^{-1}(\omega^{-1} a q_\beta^{-1} x\,|_a),$$

represents the integrated effect of the velocity and density gradients between the turning radius and the surface. The solution of (17) is then

$$\omega \int_{R_\beta}^{a} |q_\beta|\,dr = (n + \tfrac{1}{4})\pi + \theta(a, R_\beta) - \tan^{-1}(c_2/c_1), \tag{18}$$

in terms of the radial order n. We recall that (18) is appropriate to a fixed slowness p so that the phase term may either be connected to the body wave intercept time $\tau_\beta(p)$ or alternatively in a form corresponding to Nolet & Kennett (1978)

$$\omega \int_{R_\beta}^{a} |q_\beta|\,dr = \tfrac{1}{2}\omega\tau_\beta(p) = (l + \tfrac{1}{2})\chi(c), \tag{19}$$

where c is the phase velocity (a/p) and $\omega p = L \sim (l + \tfrac{1}{2})$ for large l.

Equation (18) shows us that the dispersion of the toroidal modes depends on the ratio c_2/c_1 and thus on the nature of the *SH* wavefield at the core–mantle boundary.

We can distinguish three slowness regimes:

2.1.1 An SH-wave turning point well above the core–mantle boundary (4 km/s < c < 12 km/s)

In this case the *SH* waves will be evanescent at the radius b and we may use the asymptotic approximations for Aj etc. of the type

$$\text{Aj}\,[\omega H_\beta(b)] \sim \tfrac{1}{2} q_\beta(b)^{-1/2} \exp\,(-\omega\,|H_\beta(b)|), \tag{20}$$

and then

$$\frac{c_2}{c_1} \sim \tfrac{1}{2} \exp\left(-2\omega \int_b^{R_\beta} |q_\beta|\,dr\right)\left(\frac{1 + \omega^{-1}|q_\beta|^{-1} b x}{-1 + \omega^{-1}|q_\beta|^{-1} b x}\right)\Bigg|_{r=b}, \tag{21}$$

and this will be very small. If c_2/c_1 is regarded as entirely negligible then (18) reduces to Nolet & Kennett (1978) equation (3.6) with a correction term for velocity and density gradients in the model.

2.1.2 Turning point near the core–mantle boundary (12 km/s < c < 15 km/s)

Once a turning point for *SH* waves comes close to the boundary the asymptotic development leading to (21) is no longer appropriate and the full forms of the Airy functions must be

used. If the *SH* wave just fails to turn we may take R_β to be given by $q_\beta = 0$ with the velocity distribution analytically continued beyond the core–mantle boundary as mentioned by Woodhouse (1978). The modes in this slowness range correspond to S_H diffracted body waves and we may approximate the behaviour by taking the turning radius R_β to lie at the core–mantle boundary. Then

$$\frac{c_2}{c_1} = \frac{1}{\sqrt{3}} + 0\,[\omega^{-2/3} z(b)],$$

the slight correction arising from the local velocity and density gradient at the core–mantle boundary and

$$\tfrac{1}{2}\omega\tau_\beta(p) = (n + 1/12)\,\pi + \theta(a, b), \tag{22}$$

the correction term for S_H diffracted modes depends on the velocity and density gradients throughout the mantle.

2.1.3 Reflection at the core–mantle boundary (15 km/s < c)

We now have propagating *SH* waves throughout the whole mantle and may therefore employ asymptotic approximations to the Airy functions similar to (16). There is now no turning point in the mantle for these *ScS* equivalent modes and so we recover a form similar to (18) but without the $\pi/4$ phase shift arising from a turning point

$$\omega \int_b^a |q_\beta|\, dr = \tfrac{1}{2}\omega\tau_\beta(p) = n\pi + \theta(a, b), \tag{23}$$

with the correction for gradients encompassing the whole mantle.

Thus as the phase velocity increases the phase shift in the asymptotic relation (18) for the toroidal mode eigenfrequencies remains close to $\pi/4$ until the *SH* wave turning point approaches the core–mantle boundary, the phase shift then reduces steadily through $\pi/12$ for *S* diffracted modes to zero for *ScS* equivalent modes (Fig. 1).

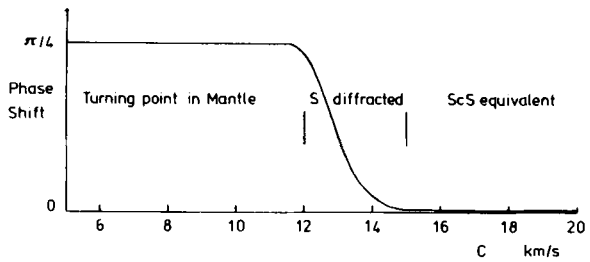

Figure 1. Pattern of phase shifts with change of mode character as the phase velocity c increases and thus slowness $p\,(= a/c)$ decreases.

2.2 A MANTLE WITH A DISCONTINUITY

We will consider initially a single discontinuity at a level $r = d$. The relation between the surface displacement $W(a)$ and that at the core–mantle boundary is given by

$$\begin{pmatrix} W(a) \\ 0 \end{pmatrix} = \mathbf{F}_T(a)\,[\mathbf{F}_T(d_+)]^{-1}\mathbf{F}_T(d_-)\,[\mathbf{F}_T(b)]^{-1} \begin{pmatrix} W(b) \\ 0 \end{pmatrix}. \tag{24}$$

By analogy with (13) we may write

$$\begin{pmatrix} W(a) \\ 0 \end{pmatrix} = \mathbf{F}_T(a) \begin{pmatrix} c_1' \\ c_2' \end{pmatrix}, \tag{25}$$

and $(c_1', c_2')^T$ will represent a modification of (14) by the interface term arising from the discontinuity

$$\begin{pmatrix} c_1' \\ c_2' \end{pmatrix} = [\mathbf{F}_T(d_+)]^{-1} \mathbf{F}_T(d_-) \begin{pmatrix} c_1 \\ c_2 \end{pmatrix}. \tag{26}$$

Any additional discontinuities will introduce similar interface terms and so a close examination of (26) will give a basis for extension to multiple discontinuities. The eigenfrequencies of the toroidal modes at fixed slowness p will be given by

$$\omega H_\beta(a) = (n + \tfrac{1}{4})\pi + \theta(a) - \tan^{-1}(c_2'/c_1'), \tag{27}$$

and we will examine the modification from the relation (18) introduced by the presence of the discontinuity. The interface term

$$[\mathbf{F}_T(d_+)]^{-1} \mathbf{F}_T(d_-) = [\mathbf{E}_\beta(d_+)]^{-1} \mathbf{K} \mathbf{E}_\beta(d_-) + 0(\omega^{-2}),$$

with (28)

$$\mathbf{K} = \begin{pmatrix} m^{-1/2} & -\omega^{-1} d(x_+ m^{1/2} - x_- m^{-1/2}) \\ -\omega^{-1} d(y_+ m^{-1/2} - y_- m^{1/2}) & m^{1/2} \end{pmatrix},$$

where $m = \mu_+/\mu_-$ and the suffices denote the upper and lower sides of the discontinuity.

In the terms $[\mathbf{E}_\beta(d_+)]^{-1}$, $\mathbf{E}_\beta(d_-)$ we need to use the expressions (9), (10) evaluated with the turning point depth appropriate to the side of the interface under consideration. The phase term $H_\beta(d_+)$ depends on the turning point radius in the analytic continuation of the velocity structure in $r > d$, whilst $H_\beta(d_-)$ depends on the true turning point radius.

To reduce the algebraic complexity we will neglect the gradient terms henceforth in the treatment of the interface effects, since they will be one order down in frequency. To this approximation

$$c_2'/c_1' = [f_{21} + f_{22}(c_2/c_1)]/[f_{11} + f_{12}(c_2/c_1)],$$

with

$$\begin{aligned} f_{11} &= m^{1/2} \mathrm{Bk}(\omega H_\beta^+) \mathrm{Aj}(\omega H_\beta^-) - m^{-1/2} \mathrm{Bj}(\omega H_\beta^+) \mathrm{Ak}(\omega H_\beta^-) \\ f_{12} &= m^{1/2} \mathrm{Bk}(\omega H_\beta^+) \mathrm{Bj}(\omega H_\beta^-) - m^{-1/2} \mathrm{Bj}(\omega H_\beta^+) \mathrm{Bk}(\omega H_\beta^-) \\ f_{21} &= -m^{1/2} \mathrm{Ak}(\omega H_\beta^+) \mathrm{Aj}(\omega H_\beta^-) + m^{-1/2} \mathrm{Aj}(\omega H_\beta^+) \mathrm{Ak}(\omega H_\beta^-) \\ f_{22} &= -m^{1/2} \mathrm{Ak}(\omega H_\beta^+) \mathrm{Bj}(\omega H_\beta^-) + m^{-1/2} \mathrm{Aj}(\omega H_\beta^+) \mathrm{Bk}(\omega H_\beta^-) \end{aligned} \tag{29}$$

and all the phase arguments are evaluated at $r = d$. In order to determine the asymptotic dispersion of the toroidal modes from (27) we have to calculate $\tan^{-1}(c_2'/c_1')$. It is convenient to do this in terms of $\tan^{-1}(c_2/c_1)$ and using a trigonometric identity (Abramowitz & Stegun 1965, section 4)

$$\tan^{-1}(c_2'/c_1') = \Phi + \tan^{-1}\left(\frac{f_{21} + (f_{22} - f_{11}) \tan\Phi - f_{12} \tan^2\Phi}{f_{11} + (f_{12} + f_{21}) \tan\Phi + f_{22} \tan^2\Phi}\right),$$

with (30)

$$\Phi = \tan^{-1}(c_2/c_1).$$

We may only simplify this relation further if we are able to use the asymptotic forms for Aj, Ak, Bj, Bk.

2.2.1 Turning point below the discontinuity

For modes with slownesses such that the *SH*-wave turning point lies below the discontinuity we may use the forms of the Airy functions corresponding to propagating waves on both sides of the interface. Then we find

$$\tan^{-1}(c_2'/c_1') = \pi/4 - \omega H_\beta^+ + \tan^{-1}\{Q \tan(\Phi + \omega H_\beta^- - \pi/4)\}, \tag{31}$$

where $Q = \mu_- q_{\beta-}/\mu_+ q_{\beta+}$. Alternatively we may cast this result in terms of the reflection coefficient for *SH* waves incident on the top of the interface, at slowness p,

$$R = (1 - Q)/(1 + Q),$$

and then

$$\tan^{-1}(c_2'/c_1') = \Phi + \omega(H_\beta^- - H_\beta^+) + \tan^{-1}\{R \cos 2(\Phi + \omega H_\beta^-)/[1 + R \sin 2(\Phi + \omega H_\beta^-)]\}. \tag{32}$$

The behaviour of (31), (32) will depend on the nature of the wavefield in the mode.

(a) Turning point in mantle

In this case (c_2/c_1) is given by (21), and if the turning point lies well above the core–mantle boundary $\tan\Phi$ will be negligible so that (32) becomes

$$\omega[H_\beta(a) - H_\beta(d_+) + H_\beta(d_-)] = (n + \tfrac{1}{4})\pi - \tan^{-1}\{R \cos 2\omega H_\beta(d_-)/[1 + R \sin 2\omega H_\beta(d_-)]\}. \tag{33}$$

Since $H_\beta(a)$, $H_\beta(d_+)$ are evaluated with the same effective turning radius we have

$$H_\beta(a) - H_\beta(d_+) = \int_d^a |q_\beta|\,dr, \quad \text{whilst} \quad H_\beta(d_-) = \int_{R_\beta}^d |q_\beta|\,dr,$$

where R_β is the radius of the turning point, and so

$$\tfrac{1}{2}\omega\tau_\beta(p) = (n + \tfrac{1}{4})\pi - \tan^{-1}[R \cos 2\omega H_\beta(d_-)/(1 + R \sin 2\omega H_\beta(d_-))]. \tag{34a}$$

The additional term arising from the presence of the discontinuity includes the interference of waves reflected above and below the discontinuity, and there is no simple ray-mode correspondence. We note that ω appears implicitly in (34a), but approximately the additional contribution depends on the radial order number n and the ratio of the tau contribution from beneath $r = d$ to the whole, i.e.

$$\upsilon = \int_{R_\beta}^d |q_\beta|\,dr \Big/ \int_{R_\beta}^a |q_\beta|\,dr.$$

If we consider small contrasts in elastic properties at the interface (i.e. $R \lesssim 0.1$) a good approximation to the dispersion behaviour is provided by

$$\tfrac{1}{2}\omega\tau_\beta(p) = (n + \tfrac{1}{4})\pi - R \cos 2\omega H_\beta^-(1 - R \sin 2\omega H_\beta^-) = (l + \tfrac{1}{2})\chi(c). \tag{34b}$$

With the further approximation of setting $\omega = 2(n + \frac{1}{4})\pi/\tau_\beta(p)$ in the perturbing term in (34b)

$$\tfrac{1}{2}\omega\tau_\beta(p) = (n + \tfrac{1}{4})\pi - R \cos 2(n + \tfrac{1}{4})\upsilon\pi(1 - R \sin 2(n + \tfrac{1}{4})\upsilon\pi), \tag{34c}$$

and thus the solotone perturbation due to the discontinuity will be periodic in radial order n but will be a more slowly varying function of p at fixed radial order.

(b) *ScS* equivalent modes

If we now consider modes equivalent to reflections from the core–mantle boundary

$$\tan^{-1}(c_2/c_1) = \Phi \simeq -\omega H_\beta(b) + \pi/4,$$

and so (27) becomes

$$\omega[H_\beta(a) - H_\beta(d_+) + H_\beta(d_-) - H_\beta(b)] = \tfrac{1}{2}\omega\tau_\beta(p) = n\pi + \tan^{-1}(R \sin 2\omega\eta/[1 + R \cos 2\omega\eta]),$$

with

$$\eta = H_\beta(d_-) - H_\beta(b) = \int_b^d |q_\beta| dr. \tag{35a}$$

We note that we have recovered a form similar to (23) but with an additional term arising from the presence of the discontinuity at $r = d$. The structure of the perturbing term is very similar to that in (33), once the phase shift associated with the reflection is taken into account. For small contrasts in elastic parameters at the interface ($R \lesssim 0.1$) we may make a similar development to (34) and obtain

$$\tfrac{1}{2}\omega\tau_\beta(p) = n\pi + R \sin 2\omega\eta(1 - R \cos 2\omega\eta). \tag{35b}$$

Once again we have an implicity relationship for ω, but we see that approximately the discontinuity term in (35a, b) depends on the ratio of the tau contribution from below the discontinuity to the whole

$$\upsilon = \int_b^d |q_\beta| dr \Big/ \int_b^a |q_\beta| dr,$$

and with the simplest approximation to the frequency $\omega = 2n\pi/\tau_\beta(p)$

$$\tfrac{1}{2}\omega\tau_\beta(p) = n\pi - R \sin 2n\upsilon\pi(1 - R \cos 2n\upsilon\pi). \tag{35c}$$

The solotone effect is again periodic in radial order but the detailed behaviour will be rather sensitive to the location of the discontinuity in the mantle through the ratio ν.

In agreement with the results of Anderssen (1977), who considered very small slownesses, 'solotone' perturbations in the dispersion relation persist for any level of contrast at the discontinuity and scale with the reflection coefficient for small contrasts.

For these *ScS* equivalent modes we may recast equation (35a) into the form

$$\tan \tfrac{1}{2}\omega\tau_\beta(p) = R \sin 2\omega\eta/(1 + R \cos 2\omega\eta),$$

which after rearrangement becomes

$$\sin\left\{\omega \int_b^a |q_\beta| dr\right\} = R \sin\left\{\omega\left[\int_b^d |q_\beta| dr - \int_d^a |q_\beta| dr\right]\right\}, \tag{36}$$

the roots of (36) then determine the asymptotic mode dispersion. This equation may alternatively be derived directly from the asymptotic development of the propagator matrices above and below the discontinuity, but this latter approach is rather difficult to extend to multiple discontinuities. Since the right-side of (36) varies more slowly with frequency than the left-side, (36) will have roots of the form

$$\tfrac{1}{2}\omega\tau_\beta(p) = (n + \gamma)\pi, \quad |\gamma| < \pi/2.$$

The 'solotone' phase shifts associated with the discontinuity in (35) can only therefore result in moving a mode branch halfway towards the next.

2.2.2 Turning point at or above the discontinuity

We are also able to consider the case where the turning point for *SH* waves lies above or at the discontinuity. In this case c_2/c_1 will be very small and so

$$\tan^{-1}(c_2'/c_1') \simeq \tan^{-1}(f_{21}/f_{11}),$$

and there will be very little contribution to (27) if the turning point lies well above $r = d$ so we have

$$\tfrac{1}{2}\omega\tau_\beta(p) = (n + \tfrac{1}{4})\pi. \tag{37a}$$

The effect of the discontinuity will only begin to be felt when the turning point approaches the discontinuity. In a similar fashion to our discussion for the core–mantle boundary the phase shift term in (37a) will diminish from $\pi/4$ towards $\pi/12$ as the turning point approaches $r = d$. For waves reflected from the jump in elastic properties we may approximate the behaviour by using the propagating asymptotic expressions for Aj etc. in $r > d_+$ and the evanescent expressions in $r < d_-$ and so obtain

$$\tan^{-1}(f_{21}/f_{11}) = \omega H_\beta(d_+) + \tan^{-1} Q - \pi/4,$$

with $Q = \mu_- |q_{\beta-}|/\mu_+ |q_{\beta+}|$, and therefore from (27) we have

$$\omega\{H_\beta(a) - H_\beta(d_+)\} = \tfrac{1}{2}\omega\tau_d(p) = n\pi + \tan^{-1} Q \tag{37b}$$

where τ_d is the tau value for reflection from the discontinuity at $r = d$. In this reflected zone we see that the phase shift is frequency independent to this asymptotic approximation, and depends purely on the variation of the reflection coefficient with slowness. At critical refraction $Q = 0$ with a corresponding phase shift of $\pi/4$ (this value would be reduced if we use the full Airy function forms). For smaller slownesses we are into the transmitted regime which has previously been discussed. The variation in the phase shift with slowness across the region of the discontinuity is sketched in Fig. 2.

2.3 MULTIPLE MANTLE DISCONTINUITIES

We now consider a model of the upper mantle with N discontinuities in elastic properties (at $r = d_j$, $j = 1, \ldots, N$) and will index them in order of increasing radius. The surface

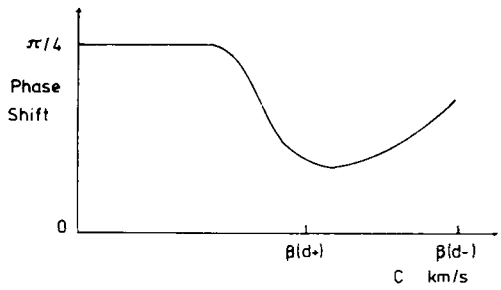

Figure 2. Pattern of phase shifts across a discontinuity occupying the phase velocity interval from $\beta(d_+)$ to $\beta(d_-)$.

displacement may now be determined from

$$\begin{pmatrix} W(a) \\ 0 \end{pmatrix} = F_T(a) \prod_{j=1}^{N} [F_T(d_j)]^{-1} F_T(d_j) \begin{pmatrix} c_1 \\ c_2 \end{pmatrix}, \tag{38}$$

with $(c_1/c_2)^T$ defined as in (13), where we have factored each of the propagator matrices between the discontinuities.

If as in Section 2.2 we ignore effects due to velocity gradients, then the analogue of (27) for the eigenfrequencies of toroidal modes at fixed slowness p is

$$\omega H_\beta(a) = (n + \tfrac{1}{4})\pi - \Phi_N, \tag{39}$$

where Φ_N is determined by the standing wave ratio above the shallowest discontinuity.

In the previous section we have established the relation (32) between the standing wave ratios (c_2'/c_1') above a discontinuity and (c_2/c_1) below, when the turning point lies beneath the interface. We may apply this relation iteratively to determine Φ_N: we work towards the surface in a cascade fashion, the standing wave ratio above one discontinuity becoming the input for a further application of (31). Thus we have

$$\Phi_j = \Phi_{j-1} + \omega [H_\beta(d_{j-}) - H_\beta(d_{j+})] + \tan^{-1}\{R_j \cos 2[\Phi_{j-1} + \omega H_\beta(d_{j-})]/(1 + R_j \sin 2[\Phi_{j-1} + \omega H_\beta(d_{j-})])\} \tag{40}$$

for $j = 1, \ldots, N$ where

$$\Phi_0 = \tan^{-1}(c_2/c_1),$$

in terms of the standing wave ratio at the core–mantle interface. R_j is the reflection coefficient for *SH* waves incident from above the jth interface, at slowness p. This iterative approach to the toroidal mode dispersion represents a generalization of the technique introduced by Tolstoy (1955) to non-uniform layering.

As we have seen from the discussions in Section 2.2, in this asymptotic approximation we need only to include the effects of discontinuities at or above the turning point for a given slowness. Thus for a turning point in the mantle the mode dispersion is given by (*cf.* (36a))

$$\tfrac{1}{2}\omega_{nl}\tau_\beta(p) = (n + \tfrac{1}{4})\pi + \Psi(\omega, p),$$

with (41a)

$$\Psi(\omega, p) = -\sum_{j=H}^{N} \tan^{-1}\left\{\frac{R_j \cos 2[\Phi_{j-1} + \omega H_\beta(d_{j-})]}{1 + R_j \sin 2[\Phi_{j-1} + \omega H_\beta(d_{j-})]}\right\} = -\sum_{j=H}^{N} \psi_j(\omega, p),$$

and $\Phi_{H-1} = 0$ if the turning point radius $R_\beta > d_H$. We may note that the phase shifts due to the various discontinuities are coupled together in the overall solotone shift $\Psi(\omega, p)$. If the individual reflection coefficients are small then an approximate development, as in (36b), may be made for the $\tan^{-1}$ terms. However, the phase shifts from the interfaces will only become additive if internal multiple reflections between interfaces are negligible. With major discontinuities present in an earth model such internal multiples can be quite significant, as may be seen, e.g. in fig. 5 of Wang *et al.* (1977), and then the full form (41a) needs to be used.

For *ScS* equivalent modes the form of (41) is modified slightly, since now all discontinuities will contribute to the phase shift. Thus we have

$$\tfrac{1}{2}\omega_{nl}\tau_\beta(p) = n\pi + \tilde{\Psi}(\omega, p),$$

and

$$\tilde{\Psi}(\omega, p) = -\sum_{j=1}^{N} \tan^{-1}\left\{\frac{R_j \cos 2[\Phi_{j-1} + \omega H_\beta(d_{j-})]}{1 + R_j \sin 2[\Phi_{j-1} + \omega H_\beta(d_{j-})]}\right\}, \tag{41b}$$

where

$$\Phi_0 = -\omega H_\beta(b) + \pi/4,$$

as in Section 2.2. In this case also the solotone shifts from the discontinuities will not in general be purely additive.

Both the expressions (41a, b) may be used for earth models containing velocity inversions provided that their use is restricted to a slowness range such that the corresponding turning points lie beneath the base of the deepest velocity inversion.

For an earth model with multiple discontinuities, (41a, b) may be used either to determine the slowness behaviour at fixed frequency or alternatively to examine frequency variation at fixed slowness. In each case we note that Ψ, $\tilde{\Psi}$ are functions of ω, p and it is convenient to work in terms of perturbations from the simplest form

$$(l + \tfrac{1}{2})\chi_1(c) = \tfrac{1}{2}\omega_{nl}\tau_\beta(p) = (n + \tfrac{1}{4})\pi, \tag{42}$$

which neglects all gradient and discontinuity effects (Pekeris 1965; Nolet & Kennett 1978). Equation (42) predicts a regular spacing of eigenfrequencies with radial order n and the additional solotone phase shifts Ψ lead to oscillating perturbations in this spacing. Roughly these perturbations will be a superimposition of periodic effects associated with individual discontinuities. At fixed frequency (41) regarded as an equation for slowness will give shifts in the apparent intercept time $\tau_\beta(p)$. 'Solotone' effects therefore arise in both radial and angular orders.

3 Group velocity and the pattern of solotone behaviour

We may summarize the various results obtained in the second section by writing

$$(l + \tfrac{1}{2})\chi(c) = \tfrac{1}{2}\omega\tau_\beta(p) = (n + \tfrac{1}{4})\pi + \Psi(\omega, p), \tag{43}$$

for phase velocity $c(= a/p)$. We have here reintroduced the notation of Nolet & Kennett (1978) since this allows a convenient treatment of group velocity. For an earth model with significant velocity and density gradients in addition to discontinuities, the phase shift Ψ will take the form

$$\Psi(\omega, p) = \sum_{j=H}^{N} \psi_j(\omega, p, d_j) + \theta(\omega, p, R_\beta),$$

where the sum is to be taken over all discontinuities which lie above the turning point for a ray with apparent velocity a/p (as in (41)). The term $\theta(\omega, p, R_\beta)$ represents the integrated effect of velocity and density gradients within the model, and for moderate gradient levels will depend on ω^{-1} and thus diminish at high frequencies.

For high-frequency modes $L = [l(l+1)]^{1/2}$ is very close to $(l + \frac{1}{2})$ so that at constant radial order n,

$$(L + \Delta L)\chi(c + \Delta c) - \Psi(L + \Delta L, c + \Delta c) = L\chi(c) - \Psi(L, c)$$

from (43), and so to first order

$$\left(\frac{\partial c}{\partial L}\right)_{n = \text{const}} = -\frac{\chi(c) - \partial_L \Psi}{L\chi'(c) - \partial_c \Psi}. \tag{44}$$

Thus the group velocity

$$\mu(c) = c + L\left(\frac{\partial c}{\partial L}\right)_{n = \text{const}} = -\frac{\chi(c) - \partial_L \Psi}{\chi'(c) - L^{-1}\partial_c \Psi}. \tag{45}$$

We may simplify this relation slightly by introducing $\chi_1(c)$, the distribution which pertains to the simplest approximation ignoring any gradient or discontinuity terms (42) so that

$$L\chi = L\chi_1 + \Psi.$$

This reduces (45) to the form

$$\mu(c) = c - \frac{\chi_1(c)}{\chi_1'(c)} - \frac{(\Psi - L\partial_L \Psi)}{L\chi_1'(c)} = \mu_1(c) - \frac{(\Psi - L\partial_L \Psi)}{L\chi_1'(c)}, \tag{46}$$

where $\mu_1(c)$ is the group velocity from the simplest approximation. The χ_1 function and its derivatives can be related to the travel time curve by

$$\chi_1(c) = \tfrac{1}{2}p^{-1}\tau_\beta(p),$$

$$L\chi_1'(c) = \tfrac{1}{2}\omega p T(p),$$

where $T(p)$ is the travel time for ray parameter p, phase velocity c. The first approximation to the group velocity

$$\mu_1(c) = X(c)/T(c)$$

is constant for fixed phase velocity, as noted by Nolet & Kennett (1978). Once allowances are made for the effects of the velocity gradients and discontinuities

$$\mu(c) = \mu_1(c) - 2c(\Psi - 2\omega\partial_\omega \Psi + c\partial_c \Psi)/[a\omega T(c)], \tag{47}$$

there will thus be fluctuations in the group velocity with frequency (and thus radial order n), at fixed phase velocity c, since Ψ and its derivatives are frequency dependent. We expect the magnitude of such fluctuations to increase in size, in general, with increasing phase velocity as may be seen in Fig. 7; the behaviour with frequency and thus radial order n is rather more complex.

With increasing phase velocity the turning point for *SH* waves penetrates further into the Earth and the effects of the discontinuities become felt in turn (see, e.g. Figs 5–7). We will restrict our attention to phase velocities for which the turning point lies beneath the deepest velocity inversion.

As the turning point approaches a discontinuity the phase shift Ψ diminishes and there will therefore be a slight decrease in the group velocity. Within the phase velocity range associated with a discontinuity the major contribution to Ψ is frequency independent (37b) and so the group velocity perturbation will depend on $[\omega T(c)]^{-1}$. Across the discontinuity $T(c)$ will correspond to a retrograde branch and will therefore diminish with increasing c, with the result that $\mu(c)$ will decrease from $\mu_1(c)$. Such drops in the group velocity associated with the discontinuities may be clearly seen in Fig. 9. However, superimposed on this behaviour will be oscillations due to overlying discontinuities.

When the turning point lies just below the kth discontinuity we may extract the dominant contribution from Ψ, which with the simplest approximation for the frequency is

$$\Psi = \tan^{-1}\left(R_k \cos\left[2(n+\tfrac{1}{4})\upsilon_k\pi\right] / \left\{1 + R_k \sin\left[2(n+\tfrac{1}{4})\upsilon_k\pi\right]\right\}\right) + \Psi',$$

where

$$\upsilon_k = \int_{R_\beta}^{d_k} |q_\beta|\,dr \Big/ \int_{R_\beta}^{a} |q_\beta|\,dr, \tag{48}$$

and R_k is the reflection coefficient at the kth discontinuity. We note that, as in the single discontinuity case, υ_k is the ratio of the tau contribution from beneath the kth discontinuity to the whole. Ψ is now frequency dependent so that there will be a rapid increase in group velocity as R_β emerges beneath d_k. When R_β is close to d_k, R_k is just less than unity so that the first term does indeed dominate, and also since υ_k will be very small the variation of Ψ with n will be slow. There will be small additional contributions from the overlying interfaces and these will be magnified in the group velocity behaviour.

Once the phase velocity c increases further and the turning point lies well below the deepest discontinuity the reflection coefficients diminish and so the contribution of an individual discontinuity to the phase shift will be fairly small. They all increase in size and so there will be rapid variations in Ψ with n. Since the size of the contributions from the various discontinuities are then comparable, there are beating phenomena with respect to n between the oscillations controlled by the various ν_j. These beating phenomena will once again be magnified in the group velocity behaviour and will be the main contribution for *ScS* equivalent modes.

4 Discontinuity effects for model 1066B

To assess the effects of discontinuities in a realistic earth model we have carried out a range of calculations of the toroidal mode dispersion for model 1066B (Gilbert & Dzeiwonski 1975) with three discontinuities, at the Moho and in the upper mantle at depths of 420 and 670 km (Fig. 3). We have considered radial orders (n) from 1 to 29 and angular orders (l) out to 700. To reduce the computation we used an l step of 5 out to angular order 300 and a step of 10 from there out to $l = 700$. Where necessary we have used quadratic interpolation between computed values, random checks show that this is not a significant source of error.

For each phase velocity c, between 5 and 20 km/s, we have constructed the best fitting relation of the form

$$(l + \tfrac{1}{2})\chi(c) = [n + \gamma(c)]\,\pi$$

to the suite of toroidal modes with that phase velocity. The $\gamma(c)$ values are given in Table 1 and we see that they broadly follow the pattern of Fig. 1 in the transition from modes with

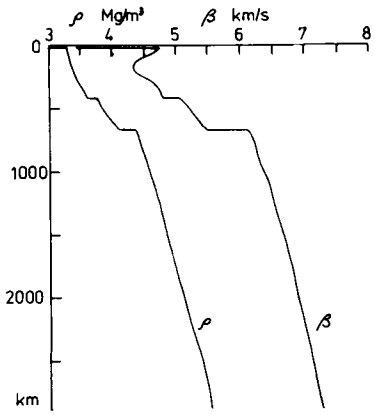

Figure 3. The earth model 1066B, showing both shear wave velocity β and density ρ.

a turning point in the mantle to *ScS* equivalent modes. The two particularly low values of $\gamma(c)$ for the upper mantle c = 5.0, 7.0 km/s correspond to turning points just above and just below a discontinuity. We note that throughout the mantle $\gamma(c)$ differs from the value of 0.25 predicted by the simplest asymptotic theory, due to gradients (e.g. near 1100 km) as well as the discontinuities.

As we have seen, the influence of the mantle discontinuities is determined by the reflection coefficients at the interfaces. In Fig. 4 we therefore show the variation of the *SH* wave reflection coefficients with phase velocity from 5–20 km/s for incidence from above the three discontinuities in model 1066B. The coefficients for the two deeper discontinuities are small for all modes bottoming in the lower mantle or reflected from the core–mantle boundary but can be sizeable at near grazing incidence. The Moho reflection coefficient is however typically greater than 0.2 so that it has a noticeable influence on the character of the solotone effect. (For model 1066A with an even more pronounced Moho, the reflection coefficient is greater than 0.4 giving rise to the possibility of marked trapping of energy in the crust.)

Table 1. Variation of phase shift $\gamma(c)$ with phase velocity c.

c (km/s)	$\gamma(c)$	Mode character
5.0	0.066	
6.0	0.341	
7.0	0.145	
8.0	0.280	Turning point in mantle
9.0	0.330	
10.0	0.340	
11.0	0.317	
12.0	0.261	
13.0	0.154	
14.0	0.090	*S* diffracted
15.0	0.038	
16.0	0.004	
17.0	−0.016	
18.0	−0.029	*ScS* equivalent modes
19.0	−0.022	
20.0	−0.055	

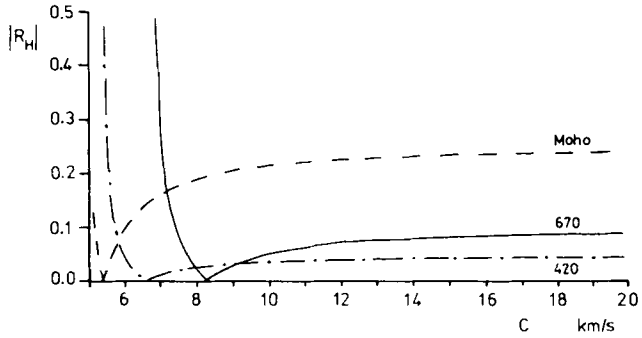

Figure 4. The variation of the *SH* wave reflection coefficients from the three mantle discontinuities in model 1066B (Moho, 420 km, 670 km) as a function of phase velocity.

In Figs 5 and 6 we consider the dispersion characteristics of model 1066B from both the direct computations and from the asymptotic results. In order to separate out the solotone variations from the regular progression of eigenfrequencies as a function of radial order n, for fixed phase velocity, we consider the phase shift $V\pi$ defined as: (a) for a turning point in the mantle (5 km/s $\leq c <$ 13.24 km/s)

$$\tfrac{1}{2}\omega_{nl}\tau_\beta(p) = [n + \tfrac{1}{4} + V(\omega, p)]\,\pi$$

and (b) for *ScS* equivalent modes (13.24 km/s $< c$) (49)

$$\tfrac{1}{2}\omega_{nl}\tau_\beta(p) = [n + V(\omega, p)]\,\pi.$$

This definition does, of course, distort the phase shift for phase velocities near 13 km/s, but is simple to use.

In Fig. 5 we show the values of V from computation of the toroidal eigenfrequencies for model 1066B; in Fig. 6 we show the calculated phase shift V_d for the cumulative effect of all the mantle discontinuities (41) using the frequencies derived from the direct computations. In addition we show the combined contribution of the 420 and 670 km discontinuities to the phase shift, so that the modifications due to the Moho may be examined. The sets of phase shifts are directly comparable and we are able to see the contribution of the discontinuities to the overall shift.

Except for small values of $n(\lesssim 8)$ where the asymptotic treatment is likely to be in error, the phase shifts in Fig. 6 are indistinguishable from those obtained by an iterative solution of equations (40) and (41), starting from the simplest approximation for the frequency.

The most obvious differences between Figs 5 and 6 occurs for small phase velocities even for large n. Even though the frequencies are rather high for radial orders above 20, the modes in this slowness range are interacting strongly with the upper mantle velocity gradients. The general form of the computed and asymptotic phase shifts are very similar, but the gradient contribution leads to an offset which diminishes with frequency and thus radial order number n. Such offsets are most noticeable for phase velocities between 6 and 9 km/s.

For a range of phase velocities from 12–16 km/s, which span the transition between a turning point in the mantle and *ScS* equivalent modes, offsets between the asymptotic phase shifts and the directly computed values occur because of the simplicity of our comparison procedure.

For the lowest radial orders the frequencies are too low for the asymptotic form to be accurate. As the frequency increases the agreement between the direct computations and the asymptotic phase shifts becomes very good indeed, once slight effects due to the nature of the wavefield are taken into consideration. Once the period is less than 45 s, gradient effects are very small (for $c > 9$ km/s) and the asymptotic curves overlie the direct calculations. For modes bottoming in the upper mantle the effects of gradients appear to be negligible at around 25 s period. Thus at high frequencies we may economically employ the simple scheme (40) and (41) to get an iterative solution for the dispersion of toroidal modes.

The results in Figs 5 and 6 correspond closely to the features discussed in the previous section, and we may use the calculations for the effect of the upper mantle discontinuities alone in Fig. 6 to examine how the phase shifts are built up. At a phase velocity of 5 km/s the turning point lies just above the 420 km discontinuity and so the sole contribution is from the Moho. By 6 km/s we have a small periodic effect from the 420 km interface and a relatively small contribution from the Moho since we are close to a null in the reflection coefficient (Fig. 4). The very slow variation for $c = 7$ km/s corresponds to a turning point just below the 670 km discontinuity, the large reflection coefficient for this interface (Fig. 4) means that its contribution swamps that from the 420 km discontinuity; there is also a significant phase shift due to the Moho. At $c = 8$ km/s the upper mantle shift is more rapidly varying but of smaller amplitude due to interaction between the two discontinuities. A noticeable beat pattern has developed on the $c = 10$ km/s plot for which the reflection coefficient (Fig. 4). The very slow variation for $c = 7$ km/s corresdponds to a turning point velocity increases, beating phenomena from the upper mantle discontinuities dominate the details of the pattern. We note that the Moho effect becomes much less rapid with n as the phase velocity increases. This is in part due to the relatively slow variation of frequency with n for large phase velocities and also to the fact that v_{Moho} will be close to unity for turning points in the lower mantle and *ScS* equivalent modes so that from (48) one could expect a slow variation of Ψ_{Moho} with n.

The group velocity behaviour (Fig. 7) to some extent mirrors the fluctuations of the phase shift, but the presence of the derivatives of the phase shift Ψ in (47) enhances the more rapid fluctuations with radial order n. It is also clear from Fig. 7 that the amplitude of the group velocity variations is increasing with increasing phase velocity as predicted by (47). For $c = 7$ km/s where the turning point lies just below the 670 km discontinuity there is a relatively smooth variation in group velocity. The behaviour is however more complex once the turning point moves away from a discontinuity and we may note the generally similar behaviour for $c = 6$ km/s, where the turning point lies between the 420 and 670 km discontinuities, and $c = 8$ km/s with a turning point at about 1300 km depth. The beating phenomena which were visible in Figs 5 and 6 are much clearer in the group velocity fluctuations and dominate for $c > 9$ km/s, i.e. for turning points in the lower mantle, *S* diffracted and *ScS* equivalent modes.

In Fig. 8 we show the group velocity for all the radial orders from 0 to 29 as a function of period from 10 to 500 s. This diagram is dominated by bands of oscillatory behaviour which we may associate with the discontinuities and strong gradient zones in model 1066B. The group velocities up to 4.8 km/s are associated with phase velocities less than 6.9 km/s (Fig. 7) and therefore correspond to modes with energy concentrated above the 670 km discontinuity. In a similar way to Kausel, Schwab & Mantovani (1977) we may separate the upper and lower parts of these oscillations. The local group velocity minima for group velocity below 4.4 km/s are associated with mode eigenfunctions concentrated above the 420 km discontinuity whilst the upper portions correspond to eigenfunctions which penetrate down to the 670 km discontinuity. The oscillatory behaviour for group velocity

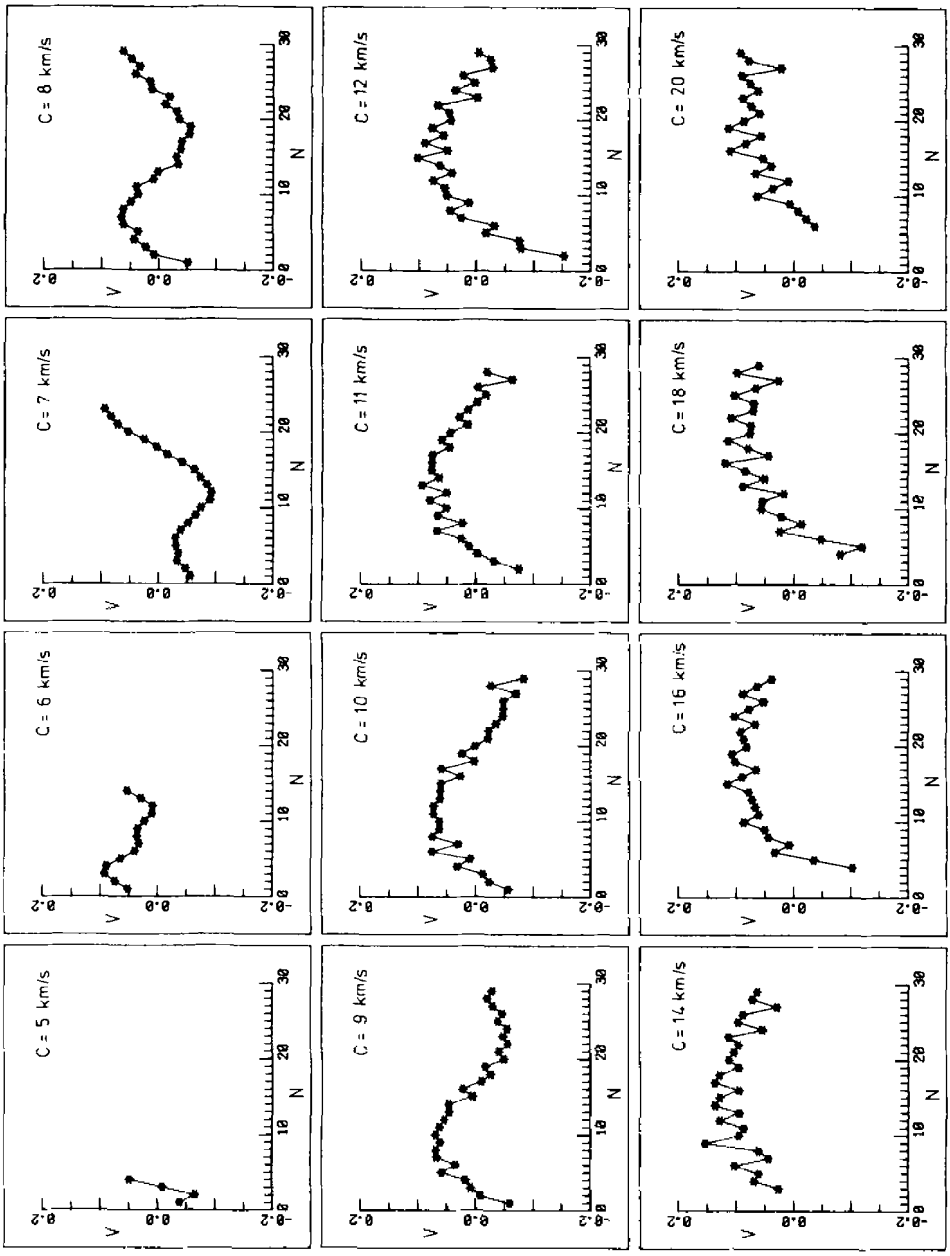

Figure 5. Phase shifts for model 1066B derived from direct calculations of toroidal mode frequencies, by numerical solution of the differential equations (4) subject to the boundary conditions (5).

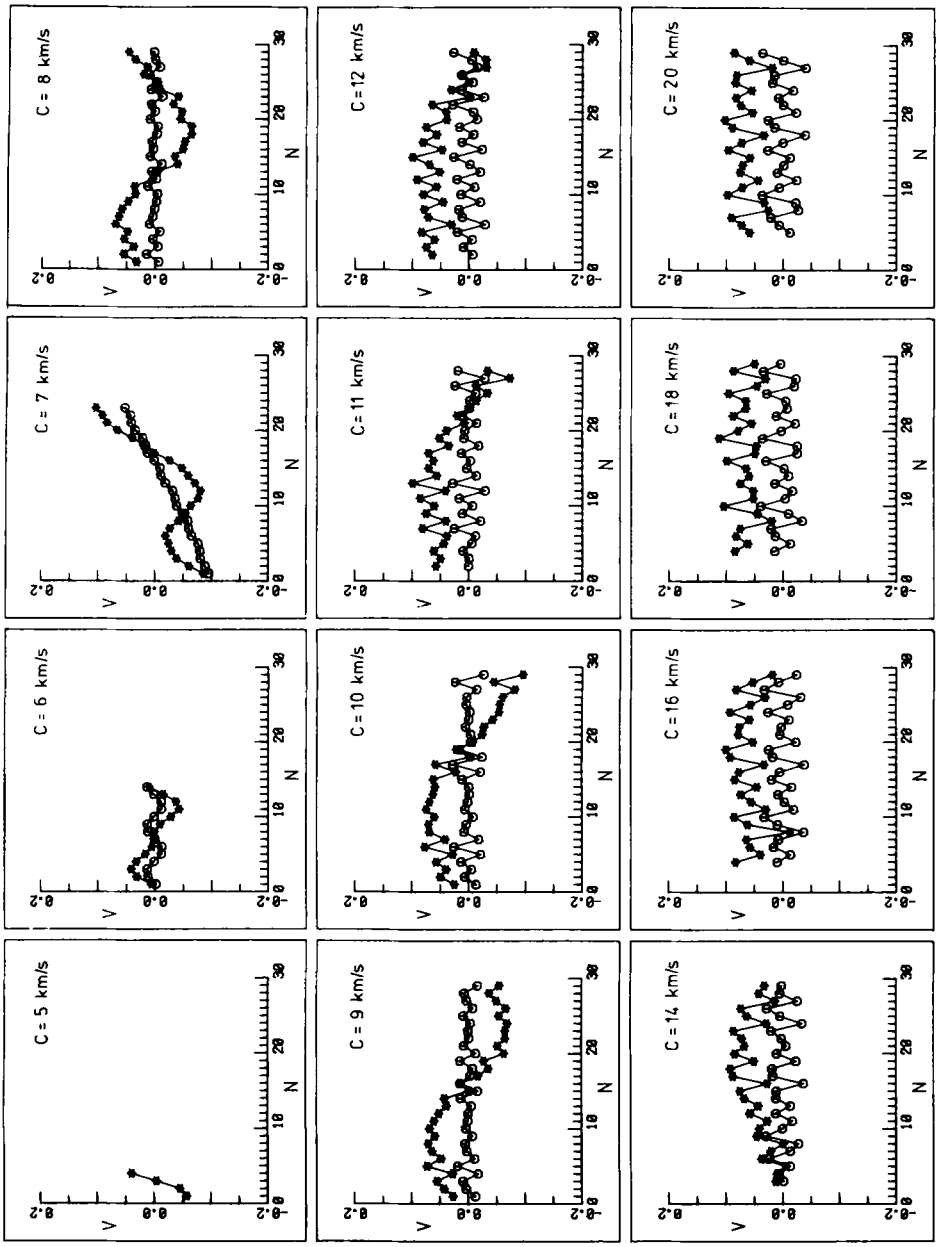

Figure 6. Phase shifts for model 1066B derived from an asymptotic treatment of discontinuity effects (equations (40) and (41)). The open symbols denote contributions from the 420 and 670 km discontinuities, whilst the solid symbols also include the Moho effects.

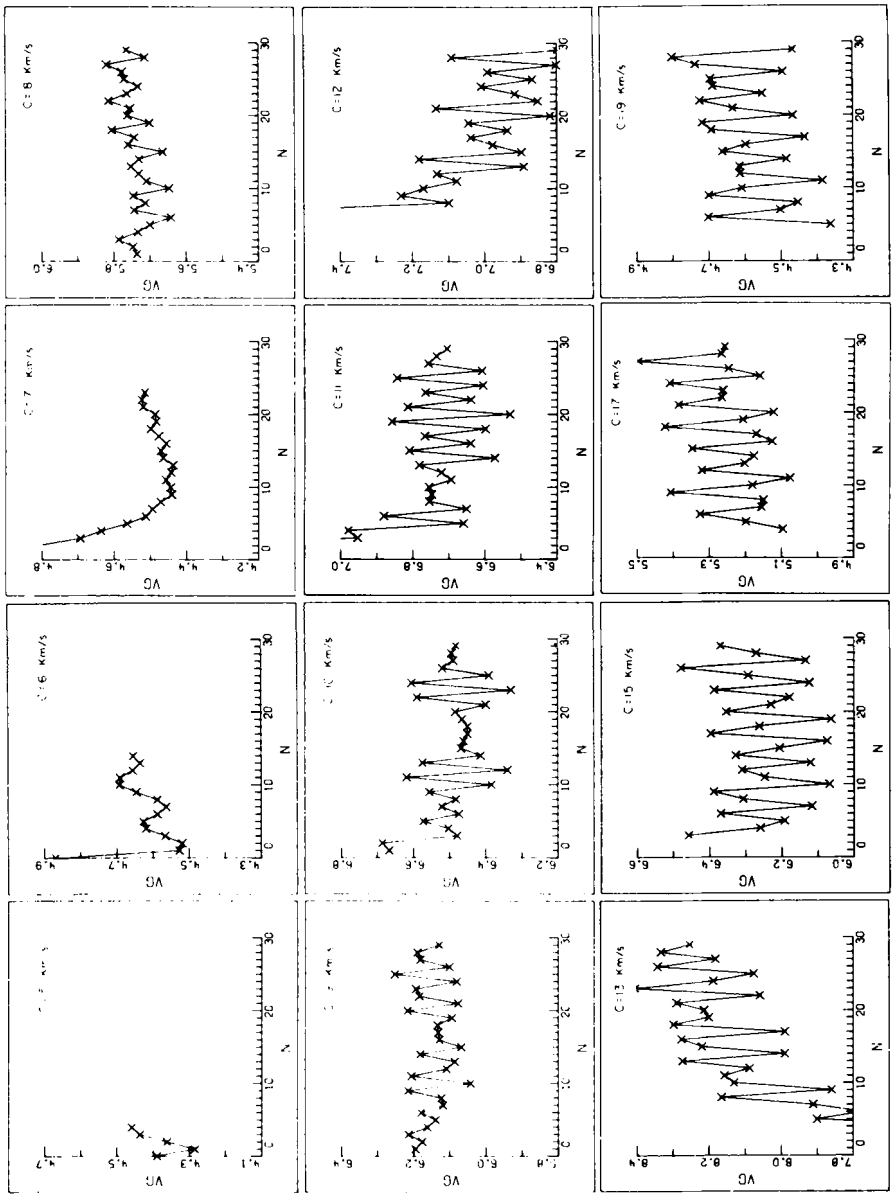

Figure 7. Group velocity (VG) behaviour as a function of radial order n for fixed phase velocity c ranging from 5.0 to 20.0 km/s.

between 5.0 and 5.6 km/s corresponds to phase velocities between 7.0 and 7.7 km/s (Fig. 7) and is associated with modes with corresponding turning points between the 670 km discontinuity and the velocity gradient zone at 1100 km. The irregularities in the group velocity above 5.6 km/s correspond to the beats between different discontinuity contributions we have already seen.

The 'solotone' effects associated with the presence of discontinuities and velocity gradients in model 1066B are summarized in Fig. 9 which shows a plot of group velocity against phase velocity for modes 7–29. Rather large deviations occur for modes 0–6 which are most sensitive to density as well as velocity structure. We recall that in the simplest approximation there would be a single group velocity for each phase velocity so that the width of the band is a measure of the size of the solotone effect. The range of phase velocities occupied by the 420 and 670 km discontinuities are indicated by shading and we see that as discussed in the previous section the group velocity decreases markedly for these regions of reflections. A similar effect, but on a larger scale may be seen for the reflected *ScS* equivalent modes for phase velocities greater than 14 km/s.

The breadth of the band of group velocities tends to increase with depth, with a rather smoother behaviour for *ScS* equivalent modes. Strong oscillations with phase velocity occur for modes with turning points between discontinuities or gradient zones. As for example for phase velocities between 5.4 and 6.1 km/s when the turning point lies between the 420 and 670 km discontinuities and between 7.0 and 7.7 km/s where turning points lie between the 670 km discontinuity and the 110 km gradient zone.

We have seen that it is only for the low radial order modes that velocity and density gradients make a significant contribution to the phase shift. Thus apart from some measure of the density contrast at discontinuities, high-frequency toroidal modes will throw little light on the density structure within the Earth.

5 Pulse formation and the solotone effect

The constructive interference conditions presented by Nolet & Kennett (1978) show that we expect pulse-like arrivals to occur by superposition of modes when the group velocity $U(c)$ is stationary with respect to L and the range is such that $x(c) = U(c)T(c)$. The presence of the additional phase shift $\Psi(\omega, c)$ due to velocity and density gradients and discontinuities (as discussed in Sections 2 and 3) will degrade the quality of pulse formation corresponding to high-order multiple S reflections.

If attention is concentrated on waves which bottom in the lower mantle or at the core–mantle boundary the S and SS arrivals will generally not be strongly affected by deep discontinuities since the travel time differences between the direct path and, e.g. waves reflected at the underside of discontinuities will be considerable. A large epicentral distance is required before the full pattern of interfering waves is established, as considered in our normal mode treatment. A shallow discontinuity such as the Moho may however produce reflections which interfere with relatively long-period pulses.

The method introduced by Brune (1964) for the determination of toroidal mode dispersion by analysis of multiple S pulses has been extensively applied by Brune & Gilbert (1974) to determine a large number of mode periods. Brune & Gilbert (1974) have correlated multiple S reflections with equal phase velocity at a pair of stations and estimated mode periods by finding the periods

$$T = \frac{t - \Delta\, dt/d\Delta}{n + T\{\phi_2(T) - \phi_1(T)\}/2\pi}, \tag{50}$$

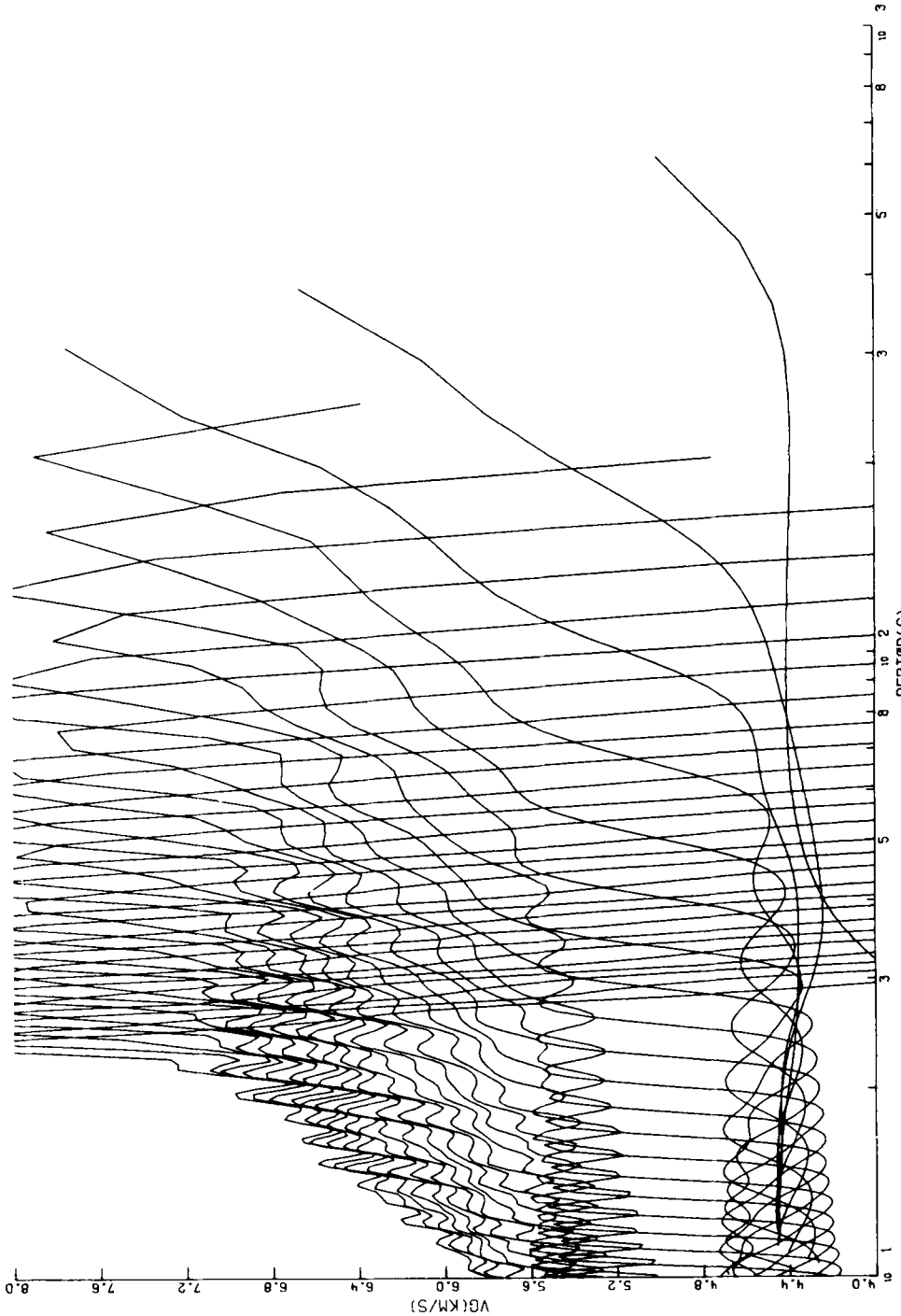

Figure 8. Group velocity (VG) as a function of period from 10 to 1000 s for modes with radial orders 0 to 29 and angular orders out to 700.

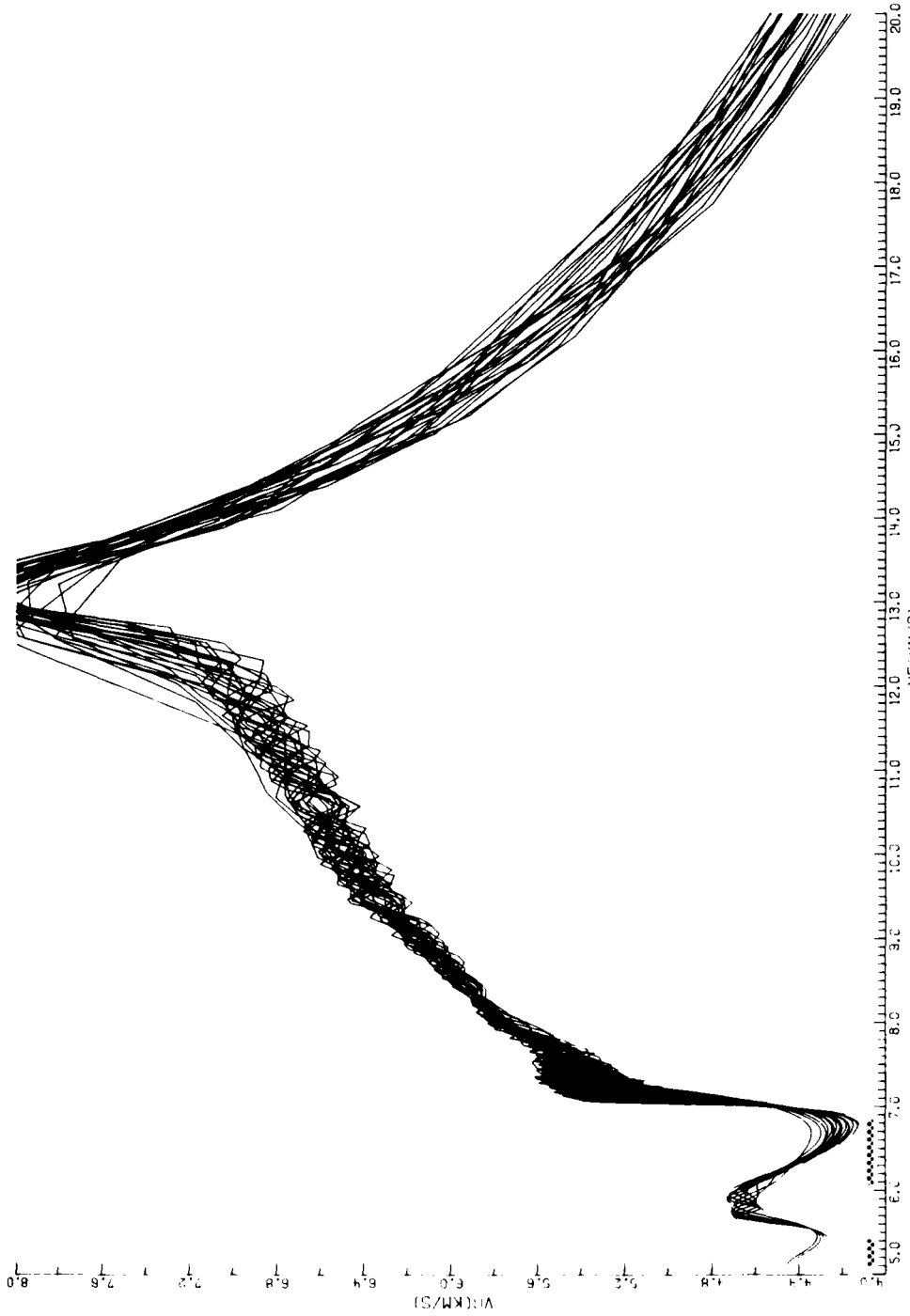

Figure 9. Group velocity (VG) as a function of phase velocity (VF), for radial orders 7–29, the width of the band of group velocities for a single phase velocity is a measure of the size of the solotone effect.

for which n is an integer. Δ is here the angular separation between the stations, t the difference in fiducial times and $\phi_1(T)$, $\phi_2(T)$ the phases of the pulses as a function of period. The angular order is estimated from

$$(l + \tfrac{1}{2}) = 2\pi T^{-1} dt/d\Delta.$$

Since it is very difficult to obtain station pairs exactly positioned to receive successive multiple S reflections a number of corrections have to be made and these are based on the assumption that the group velocity is $U(c) = \Delta/t$.

If we compare (50) with our asymptotic expressions (49) for the normal mode period

$$T = \frac{\tau_\beta(p)}{n + \tfrac{1}{4} + V(T, p)} \tag{51}$$

we see that we have, as expected, a very close correspondence. The estimated intercept time $t - \Delta dt/d\Delta$ in (50) is likely to be a good estimate of $\tau_\beta(p)$ since the velocity structure is already quite well known and estimates of τ are insensitive to first-order errors in p (Brune 1964). The principal source of error in (50) is therefore likely to be the extent to which the estimated phase shift $\tfrac{1}{2}T\{\phi_2(T) - \phi_1(T)\}$ is equivalent to $[V(T, p) + \tfrac{1}{4}]\pi$. Small errors in the estimated angular order may also arise from deviations in the group velocity but this should not exceed one place in l if the stations are well chosen.

For low-order multiple S reflections (in particular S and SS) the time separation between the main pulses and any phases arising by interaction with the upper mantle discontinuities is sufficiently large that for a reasonable time window about the main pulse the upper mantle phases will not appear. This means that the estimated phase shift $\tfrac{1}{2}T\{\phi_2(T) - \phi_1(T)\}$ from correlations between multiple S reflections will not include any phase shift due to upper mantle discontinuities. Thus as noted by Wang *et al.* (1977) the estimated toroidal mode periods will be biased towards a smooth upper mantle. The effect which has been neglected is however rather small.

We take the discontinuities in the upper mantle model 1066B as estimates of the likely contrasts in elastic parameters at major upper mantle discontinuities. Then from the results in Fig. 5 we may estimate the errors associated with the neglect of these phase shifts. Over the range of phase velocities from 8–20 km/s the upper mantle shift satisfies

$$|V_{\mathrm{UM}}(T, p)| < 0.04$$

and so from (51) the relative error in mode period from Brune's (1964) method

$$|\delta T_{\mathrm{UM}}/T| < 0.04/n \tag{52}$$

at radial order n. Thus for radial order 10 we would have less than 0.4 per cent relative error dropping to 0.1 per cent by radial order 40. Significant error from this cause is therefore only likely for small radial orders.

The most likely cause of contamination of mode periods arises when different interference conditions are satisfied in the two pulses analysed. This is most likely to occur when interfering phases are generated at the base of the crust, so that complications will ensue if the two stations used in the analysis are situated on rather different crustal structures. We may obtain an upper bound on such errors by assuming that only one station record includes all phases generated by the Moho discontinuity. From Fig. 6 the Moho contribution to the overall phase shift for phase velocities between 8 and 20 km/s satisfies

$$|V_{\mathrm{Moho}}(T, p)| < 0.1$$

and so the corresponding relative error in mode period is

$$|\delta T_{\text{Moho}}/T| < 0.1/n. \tag{53}$$

If both station records include some Moho phases then this relative error will be reduced but it is at least likely to be comparable to the error arising from the neglect of the effects of deeper discontinuities (52). The size of the error in (53) increases with the parameter contrast assumed at the Moho and would be somewhat larger for model 1066A, for example.

All these sources of *systematic* error in Brune's (1964) method for determining toroidal model dispersion decrease in size with increasing radial order n. This unfortunately just reflects the decrease in additional information content for high-frequency modes. The size of the errors associated with the neglect of discontinuity effects suggests that the relative errors ascribed to the mode periods determined by Brune & Gilbert (1974), which were employed in the inverse of Gilbert & Dzeiwonski (1975), may be unduly optimistic.

References

Abramowitz, M. & Stegun, I. A., 1965. *Handbook of Mathematical Functions*, Dover, New York.

Anderssen, R. S., 1977. The effect of discontinuities in density and shear velocity on the asymptotic overtone structure of torsional eigenfrequencies of the Earth, *Geophys. J. R. astr. Soc.*, **50**, 303–309.

Anderssen, R. S. & Cleary, J. R., 1974. Asymptotic structure in torsional free oscillations of the Earth – I. Overtone structure, *Geophys. J. R. astr. Soc.*, **39**, 241–268.

Brune, J. N., 1964. Travel times, body waves and normal modes of the Earth, *Bull. seism. Soc. Am.*, **54**, 2099–2128.

Brune, J. N. & Gilbert, F., 1974. Toroidal overtone dispersion from correlations of *S* to *SS* waves, *Bull. seism. Soc. Am.*, **64**, 313–320.

Gilbert, F. & Backus, G. E., 1966. Propagator matrices in elastic wave and vibration problems, *Geophysics*, **31**, 326–332.

Gilbert, F. & Dziewonski, A. M., 1975. An application of normal mode theory to the retrieval of structural parameters and source mechanisms from seismic spectra, *Phil. Trans. R. Soc. Lond. A*, **278**, 187–269.

Kennett, B. L. N. & Woodhouse, J. H., 1978. On high-frequency spheroidal modes and the structure of the upper mantle, *Geophys. J. R. astr. Soc.*, **55**, 333–350.

Kausel, E. G., Schwab, F. & Mantovani, E., 1977. Oceanic *Sa*, *Geophys. J. R. astr. Soc.*, **50**, 407–440.

Lapwood, E. R., 1975. The effect of discontinuities in density and rigidity on torsional eigenfrequencies of the Earth, *Geophys. J. R. astr. Soc.*, **40**, 453–464.

Nolet, G. & Kennett, B. L. N., 1978. Normal mode representations of multiple ray reflections in a spherical earth, *Geophys. J. R. astr. Soc.*, **53**, 219–226.

Pekeris, C. L., 1965. Asymptotic theory of the free torsional oscillations of the earth, *Proc. Nat. Acad. Sci. USA*, **53**, 1254–1257.

Tolstoy, I., 1955. Dispersion and simple harmonic sources in wave ducts, *J. Accoust. Soc. Am.*, **27**, 897.

Wang, C., Gettrust, J. F. & Cleary, J. R., 1977. Asymptotic overtone structure in eigenfrequencies of torsional normal modes of the Earth: a model study, *Geophys. J. R. astr. Soc.*, **50**, 289–302.

Woodhouse, J. H., 1978. Asymptotic results for elastodynamic propagator matrices in plane stratified and spherically stratified earth models, *Geophys. J. R. astr. Soc.*, **54**, 263–280.

Appendix: the gradient matrix T

Following Woodhouse (1978)

$$\mathbf{T}(r) = \begin{pmatrix} 0 & z - q_\beta^2 y \\ y & 0 \end{pmatrix},$$

with

$$z(r) = -r^{-2}(2 + \tfrac{1}{2}r\partial r\rho/\rho + r\partial r\beta/\beta + \tfrac{1}{2}r\partial r^2\phi_\beta/\partial r\phi_\beta),$$

$$y(r) = \tfrac{1}{2}r^{-1}\,\mathrm{sgn}\,(q_\beta^2)\,|q_\beta|^{-1}\int_{R_\beta}^{r}|q_\beta|^{-1}F(r)\,dr,$$

and

$$F(r) = r^{-3}\,[\tfrac{3}{4}(r\partial r^2\phi_\beta/\partial r\phi_\beta)^2 - \tfrac{1}{2}(r^2\partial r^3\phi_\beta/\partial r\phi_\beta) + \tfrac{1}{4}(r\partial r\rho/\rho)^2$$
$$- \tfrac{1}{2}r^2\partial r^2\rho/\rho - r^2\partial r^2\beta/\beta - r\theta r\rho/\rho)(\partial r\beta/\beta) - 4r\partial r\beta/\beta - 2r\partial r\rho/\rho].$$

For convenience we have often set

$$x = z - q_\beta^2 y,$$

in the body of the text.